

PALACKY UNIVERSITY OLOMOUC
FACULTY OF NATURAL SCIENCES

Department of Optics



**Ultra stable Mach-Zehnder interferometer
for quantum computing**

BACHELOR THESIS

Ester Doláková
2011

PALACKY UNIVERSITY OLOMOUC

FACULTY OF NATURAL SCIENCES

Department of Optics



Ultra stable Mach-Zehnder interferometer for quantum computing

BACHELOR THESIS

Author:	Ester Doláková
Study programme:	B1701 Physics
Field of study:	Optics and optoelectronics
Form of study:	Full - time
Supervisor:	Mgr. Michal Mičuda
Co - supervisor:	Mgr. Miroslav Ježek, Ph.D.

UNIVERZITA PALACKÉHO V OLOMOUCI

PŘÍRODOVĚDECKÁ FAKULTA

Katedra optiky



Vysoce stabilní Machův-Zehnderův interferometr pro kvantové počítání

BAKALÁŘSKÁ PRÁCE

Autor:

Ester Doláková

Studijní program:

B1701 Fyzika

Studijní obor:

Optika a optoelektronika

Forma studia:

Prezenční

Vedoucí práce:

Mgr. Michal Mičuda

Konzultant:

Mgr. Miroslav Ježek, Ph.D.

Bibliographical identification

Author's first name and surname:	Ester Doláková
Title:	Ultra stable Mach-Zehnder interferometer for quantum computing
Type of thesis:	Bachelor
Supervisor:	Mgr. Michal Mičuda
Co - supervisor:	Mgr. Miroslav Ježek, Ph.D.
Years of presentation:	2011
Number of pages:	21
Number of appendices:	1
Language:	English

Keywords: Mach-Zehnder interferometer, interferometer stabilization, polarization of light, quantum computing

Bibliografická identifikace

Jméno a příjmení autora:	Ester Doláková
Název:	Vysoce stabilní Machův-Zehnderův interferometr pro kvantové počítání
Typ práce:	Bakalářská
Vedoucí práce:	Mgr. Michal Mičuda
Konzultant:	Mgr. Miroslav Ježek, Ph.D.
Rok obhajoby práce:	2011
Počet stran:	21
Počet příloh:	1
Jazyk:	Anglický

Klíčová slova: Machův-Zehnderův interferometr, stabilizace interferometru, polarizace světla, kvantové počítání

Declare

I declare that I have created Bachelor Thesis "Ultra stable Mach-Zehnder interferometer for quantum computing" on my own under the guidance of Mgr. Michal Mičuda by using theoretical resources, which are referred to in the list of literature. I agree with the further usage of this document according to the requirements of the Department of optics.

Acknowledgement

My thanks go to my supervisor, Mgr. Michal Mičuda, for his help with solving the experimental and theoretical problems, for his advice, support and great patience. I would also like to express my gratitude to Mgr. Miroslav Ježek, Ph.D., members of Quantum Optics Laboratory and Department of Optics for its support. Last but not least I would like to thank my close family for their support and patience.

Abstract

We experimentally realized inherently stable Mach-Zehnder interferometer. We utilized displaced Sagnac construction and reached passive phase stability during 2500 seconds with phase shift less than 2 degrees. We measured the visibility for different input polarization states and reached more than 99.9% for the horizontal and vertical polarization state in the first output port. We reached more than 97% and 92%, for the horizontal and the vertical polarization state, respectively, in the second output port.

Contents

1	INTRODUCTION	1
2	THEORY	2
2.1	Jones notation	2
2.2	Matrix description of beam splitter	4
2.3	Characterization of Mach-Zehnder interferometer	4
2.4	Matrix description of Mach-Zehnder interferometer	4
2.5	Evaluating methods of long-time stability	8
3	EXPERIMENT	10
3.1	Half wave plate calibration	10
3.2	Beam splitter characterization	11
3.3	Mach-Zehnder interferometer	13
3.4	Long-time phase stability	16
4	CONCLUSION	18
5	APPENDIX	19

1 INTRODUCTION

The interferometer is an optical instrument where the input wave is divided into two or more waves by a beam splitter (BS). Waves reflect on mirrors and they are merged at one point where they interfere. The most common types of interferometers are Michelson, Sagnac and Mach-Zehnder. The Michelson interferometer is often used for measuring the wavelength of light [1] or measuring extremely short distances. The Sagnac interferometer is very sensitive to its tilting and therefore is often used into gyroscopes [2]. The Mach-Zehnder (MZ) interferometer is used in biosensors and in interferometer microscopy for its highly sensitivity to changes of the refractive index [3, 4]. The next utilization of the MZ is as a quantum gate which is part of quantum processor. Our experimental realized MZ interferometer will be also part of the quantum gate, especially Toffoli gate. The Toffoli gate is a three qubit quantum gate that flips the logical state of the "target" qubit conditional on the logical state of two "control" qubits. We realize MZ interferometer and characterize it by visibility and its long-time phase stability. To ensure the longest passive phase stability the displaced Sagnac construction is employed.

This work is divided into three sections. The first part, Theory, covers the Jones notation, matrix description of important optical elements, the visibility definition and the MZ interferometer characterization. We also give there brief description of two methods exploited for measuring the long-time phase stability.

The section Experiment describes experimental realization of the MZ interferometer including the half wave plate calibration, measuring the beam splitter parameters, MZ visibility and the long-time phase stability. There is discussed the measured visibility dependence on the splitting ratio of the beam splitter and on the polarization state of the input beam. We also compare the measured visibilities with and without spatial filtering by the single mode optical fiber with the theoretical values.

The main results of this work and future use of the realized MZ interferometer are reviewed in the part Conclusion. Bibliography and Appendix with setup picture are given at the end. The bachelor work and all supporting materials are included in the electronic form on the attached CD.

2 THEORY

2.1 Jones notation

The polarized light which radiates along z-axis can be fully described by Jones vector

$$J = \begin{pmatrix} \cos \vartheta \\ \sin \vartheta \cdot e^{i\delta} \end{pmatrix}, \quad (1)$$

where $\cos \vartheta$ and $\sin \vartheta$ are normalized amplitudes of the horizontal and vertical polarization vector component, respectively. In the case of the linearly polarized light, ϑ is the angle between the polarized wave and x-axis and δ is the phase difference between amplitudes [6].

There are two significant polarization states, the linear and circular polarization. To reach the significant polarization state, we change the value of angles δ and ϑ in the equation (1). The required specific angles δ , ϑ for significant polarization states are mention in the Table 1.

polarization state	δ	$\vartheta+2m\pi$	vector	notation	
linear polarization	0	0	$\begin{pmatrix} 1 \\ 0 \end{pmatrix}$	horizontal	H
		$\pi/2$	$\begin{pmatrix} 0 \\ 1 \end{pmatrix}$	vertical	V
		$\pi/4$	$\frac{1}{\sqrt{2}} \begin{pmatrix} 1 \\ 1 \end{pmatrix}$	diagonal	D
		$7\pi/4$	$\frac{1}{\sqrt{2}} \begin{pmatrix} 1 \\ -1 \end{pmatrix}$	antidiagonal	A
circular polarization	$\pi/2$	$\pi/4$	$\frac{1}{\sqrt{2}} \begin{pmatrix} 1 \\ i \end{pmatrix}$	right-handed	R
	$-\pi/2$		$\frac{1}{\sqrt{2}} \begin{pmatrix} 1 \\ -i \end{pmatrix}$	left-handed	L

Table 1: Significant states of the polarization. The parameter $m \in N$.

The optical anisotropic medium can be described by the transformation matrix in the form of

$$T = \begin{pmatrix} A & B \\ C & D \end{pmatrix}, \quad (2)$$

where elements A, B, C, D describe the optical medium and the matrix determinant is equal to one.

The output polarization state J_{out} reads

$$J_{out} = T \cdot J_{in}, \quad (3)$$

where J_{in} is the Jones vector of the input state.

Before we mention the components that change the polarization state of light we should start with mention rotation matrix. The rotation matrix is responsible for rotating the reference frame by the angle β and its matrix form is

$$R(\beta) = \begin{pmatrix} \cos \beta & \sin \beta \\ -\sin \beta & \cos \beta \end{pmatrix}. \quad (4)$$

The most common components that change polarization states are the polarizer and retarder. The linear polarizer projects an arbitrary polarization state into the linear polarization and its matrix form is

$$T = \begin{pmatrix} 1 & 0 \\ 0 & 0 \end{pmatrix}. \quad (5)$$

With the help of equations (4) and (5) we can obtain the matrix representation of the polarizer rotated about angle β

$$T(\beta) = R(-\beta) \cdot T \cdot R(\beta) = \begin{pmatrix} \cos^2 \beta & \sin \beta \cos \beta \\ \sin \beta \cos \beta & \sin^2 \beta \end{pmatrix}. \quad (6)$$

The retarder can change the polarization state and is described by matrix

$$T(\Gamma) = \begin{pmatrix} 1 & 0 \\ 0 & e^{-i\Gamma} \end{pmatrix}. \quad (7)$$

There are two distinct cases of retarders according to the phase Γ . The first is the **half wave plate**, where $\Gamma = \pi$. The half wave plate rotates the direction of the linear polarization. The second case is the **quarter wave plate**, where $\Gamma = \pi/2$. This wave plate can change the linear polarization to the circular polarization and vice versa.

With the help of equations (4) and (7) we get the retarder rotated by angle β . The matrix form is

$$T(\beta, \Gamma) = \begin{pmatrix} \cos^2 \beta + e^{-i\Gamma} \cdot \sin^2 \beta & (1 - e^{-i\Gamma}) \cdot \sin \beta \cos \beta \\ (1 - e^{-i\Gamma}) \cdot \sin \beta \cos \beta & \sin^2 \beta + e^{-i\Gamma} \cdot \cos^2 \beta \end{pmatrix}. \quad (8)$$

2.2 Matrix description of beam splitter

We used the two-mode description of optical elements and beam transformations up to now. From this point on we will use the four-mode description because we will work with the two spatial modes and two polarization modes.

The lossless BS is characterized with transmission coefficients t_H , t_V and reflectance coefficients r_H , r_V , where the subscript H denotes the horizontal polarization state and the subscript V denotes the vertical polarization state. The following equations hold for transmission and reflectance coefficients

$$|t_H|^2 + |r_H|^2 = 1, \quad |t_V|^2 + |r_V|^2 = 1. \quad (9)$$

The matrix description of the BS has a form

$$BS = \begin{pmatrix} t_H & 0 & r_H & 0 \\ 0 & t_V & 0 & r_V \\ -r_H & 0 & t_H & 0 \\ 0 & -r_V & 0 & t_V \end{pmatrix}. \quad (10)$$

2.3 Characterization of Mach-Zehnder interferometer

There are two important criteria for MZ interferometer - the visibility and its long-time phase stability. The standard definition for visibility [7] is

$$VIS = \frac{I_{max} - I_{min}}{I_{max} + I_{min}}, \quad (11)$$

where I_{max} is maximum and I_{min} is minimum of the intensity of the output port.

The visibility in the MZ interferometer mainly depends upon the spatial and polarization overlap and splitting ratio of the BSs.

The second criterium for our realized MZ interferometer is its long-time phase stability. We will try to meet this requirement with the utilization the construction of the displaced Sagnac interferometer.

2.4 Matrix description of Mach-Zehnder interferometer

The most common realization of the MZ interferometer consists of two BSs and two mirrors, see Figure 1a). The input beam is divided on the first BS and each beam reflects from the different mirror. Beams meet in the second BS where they interfere. Each of beams can feel different phase fluctuation because they are reflected by different

mirrors. It influences the interference and causes for example the visibility and stability decreasing.

Our realization of the MZ interferometer uses displaced Sagnac architecture, see Figure 1b). The interferometer consists of one BS and three mirrors. The input beam is divided on the BS and both beams are reflected from same mirrors. The MZ interferometer can be passively phase stable for long-time because both beams feel the same phase changes.

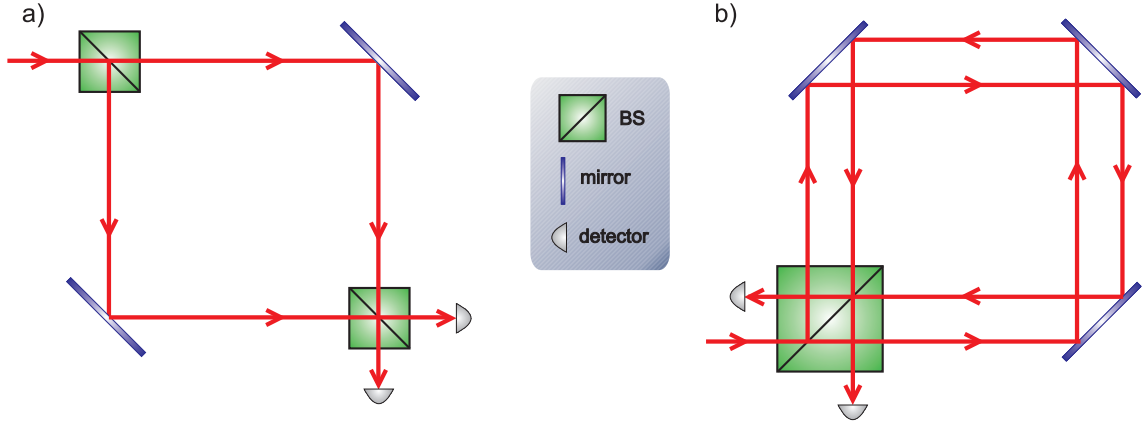


Figure 1: a) Standard realization of the MZ interferometer. b) Our realization of the MZ interferometer using displaced Sagnac architecture.

The MZ interferometer is characterized by its visibility. To calculate it we need the minimum and maximum intensity in one output port. We can reach these values by changing the phase. The matrix description of the phase difference between interferometer arms is

$$\Phi = \begin{pmatrix} e^{i\varphi} & 0 & 0 & 0 \\ 0 & e^{i\varphi} & 0 & 0 \\ 0 & 0 & 1 & 0 \\ 0 & 0 & 0 & 1 \end{pmatrix}, \quad (12)$$

where φ is phase between arms in the MZ interferometer.

Both realizations can be described by the same matrix description

$$OUT = BS_2 \cdot \Phi \cdot BS_1 \cdot IN, \quad (13)$$

where OUT is the output state, BS_1 is the first beam splitter, Φ is the phase, BS_2 is the second beam splitter and IN is the input state. We use single BS in our realization, therefore the BS_1 and BS_2 are same. The input state IN is described by the vector 1x4 where the

first two elements characterize the input state for the first spatial mode and the second two elements characterize the input state for the second spatial mode. Each spatial mode consists of two polarization modes.

The visibility mainly depends on the splitting ratio of BSs and the spatial and polarization overlap. We assume the perfect spatial overlap and no losses in our consideration. We carried out the simulation of the visibility dependence on the splitting ratio of BSs and the visibility dependence on the input polarization state.

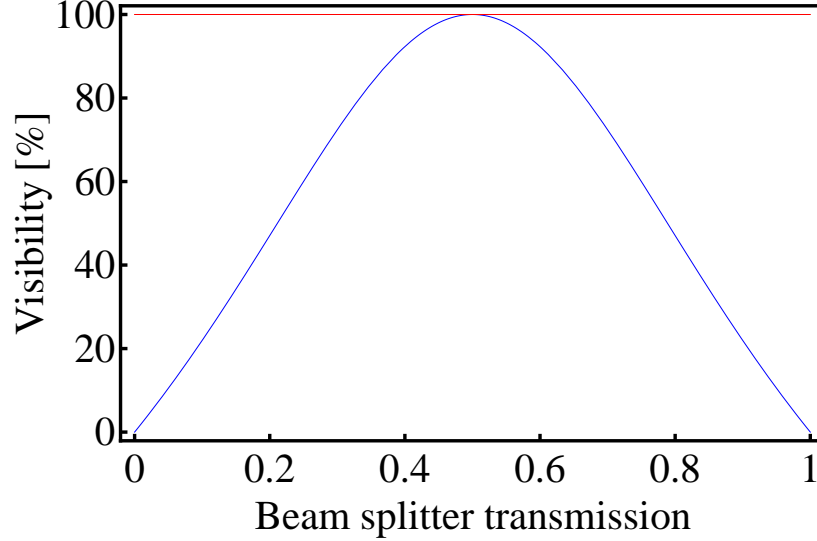


Figure 2: The visibility dependence on the transmissivity $|t|^2$ of the BS. The red curve shows the visibility in the first output port P1 and the blue curve shows visibility in the second output port P2.

We simulate the visibility dependence on BSs' splitting ratio, see Figure 2. The splitting ratio of BSs is characterized by the transmissivity $|t|^2$. The visibility in the first output port P1 is always unity and there is no dependence on the splitting ratio of BS. On the other hand the visibility in the second output port P2 depends on the splitting ratio of BS. We would reach the unity visibility for the second output port P2 if the splitting ratio is 50/50.

We investigate the visibility dependence on the input polarization state, see Figure 3. We assume the actual BS splitting ratio 53/47 for all polarization state. We chose this splitting ratio of BS because the standard manufacture's specification is $50/50 \pm 3\%$. The red curve shows the unity visibility in the first output port P1 and the blue curve represents the visibility in the second output port P2 where the visibility is 99.28%.

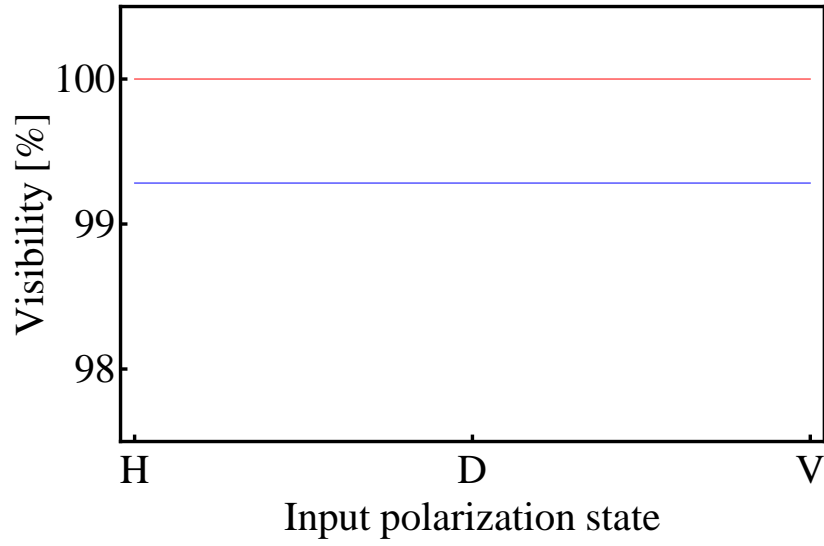


Figure 3: The visibility dependence on the input polarization state. We assume the same splitting ratio of the BS for all polarization states. H - horizontal, D - diagonal, V- vertical polarization state. The red curve represents the visibility in the first output port P1 and the blue curve represents the visibility in the second output port P2.

We also simulate the visibility dependence on the BS splitting ratio which is dependent on the polarization state, see Figure 4. We assume that BS splitting ratio is 50/50 for the horizontal polarization state and 53/47 for the vertical polarization state.

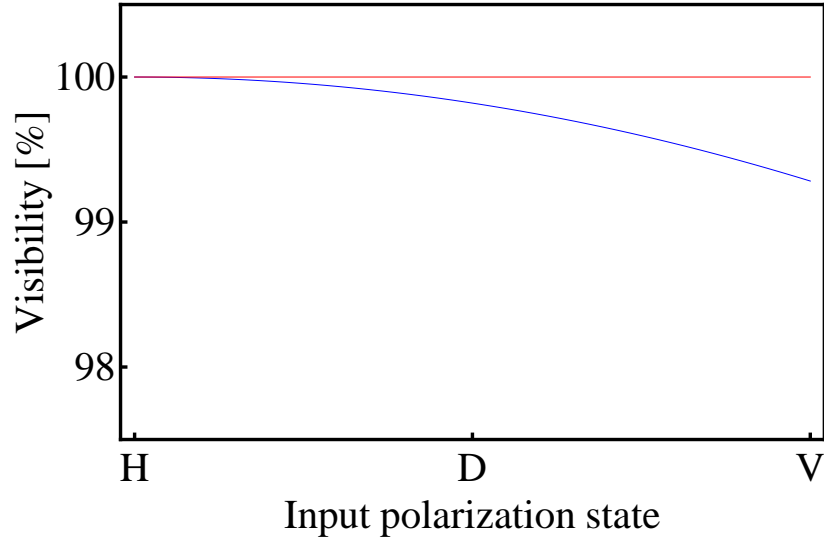


Figure 4: The visibility dependence on the input polarization state where BS splitting ratio is 50/50 for the horizontal and 53/47 for the vertical polarization state. H - horizontal, D - diagonal, V- vertical polarization state. The red curve represents the visibility in the first output port P1 and the blue curve represents the visibility in the second output port P2.

The red curve represents unity visibility in the first output port P1 and the blue curve represents the visibility in the second output port P2, which starts with the visibility of 100% for the horizontal polarization state and approaches to 99.28% for the vertical polarization state.

We can clearly see from Figures 3 and 4 that the visibility in the first output port P1 is always unity and there is no visibility dependence on the splitting ratio of the BS. On the other hand visibility in the second output port P2 is affected by splitting ratio of the BS.

2.5 Evaluating methods of long-time stability

We use two evaluating methods for the measured data of the long-time phase stability. The first method is the Allan variance. This method gives us information for how long we should perform one particular measurement step to be affected by noise as low as possible. The principle of this method is: Measure the data for time t , then divide the time t into n intervals with length τ . The next step is to calculate average value in each interval τ . Subtract the average value in the interval τ_i from average value in the interval τ_{i+1} . Square

it, sum it up and take a square root of the result. This process is described by equation

$$AVAR(\tau) = \sqrt{\frac{1}{2 \cdot (n-1)} \sum_{i=1}^n (y_{i+1}(\tau) - y_i(\tau))^2}, \quad (14)$$

where *AVAR* is Allan standard deviation, τ is the time interval, y_i is the average value in the time interval τ_i , [8].

The Average Maximum Deviation (AMD) method shows how the phase shifts in the specific time interval. The principle of the AMD method is: Measure the data for time t , then divide time t into n intervals with length τ_i . Calculate average values in each interval τ_i . Then find the maximum deviation from the average value in the interval τ_i and take absolute value of it. Sum up maximum deviations and divide by n . This process is described by equation

$$AMD(\tau_i) = \frac{1}{n} \sum_{i=1}^n \text{Max}|y_i(\tau_i) - x_{ij}|, \quad (15)$$

where y_i is the average value in the time interval τ_i and x_{ij} is measured value in interval τ_i .

3 EXPERIMENT

3.1 Half wave plate calibration

An arbitrary linear polarization state of light can be created by using the linear polarizer and half wave plate. It is necessary to know how we should rotated the half wave plate to get the required polarization state. We ensure the correct operation of the half wave plate by its calibration. The goal of calibration process is to find the optical axes of the half wave plate.

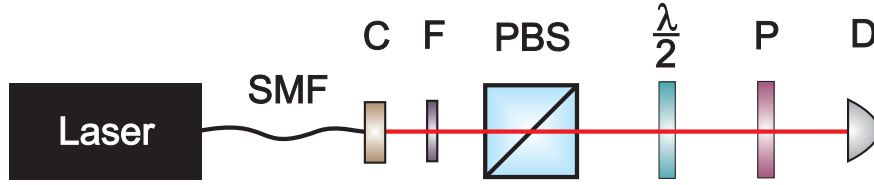


Figure 5: SMF - single mode optical fiber, C - coupler, F - filter, PBS - polarized beam splitter, $\frac{\lambda}{2}$ - half wave plate, P - linear polarizer, D - detector.

The Figure 5 shows our experimental setup. The source of linearly polarized light consists of the laser diode (OZ optics, FOSS-01-3S-5/125-810-S-1, s.n.: 97470-1) coupled into single mode optical fiber SMF (Nufern, HP780) and the linear polarizer PBS (Ekspla, E71011PZ6). The source radiates light at 816 nm wavelength with 3 nm full width half maximum (FWHM). Components employed in the setup were designed for 814 nm, therefore the narrow filter F with FWHM 2 nm (Andover Corporation, PIN: ANDV10640 AM-66377) was used. Next components are the lambda half wave plate (Ekspla, 460-4214) and linear polarizer P (Thorlabs, LPVIS100).

The PBS transmits the horizontal polarization state and the polarizer P is set to transmit the vertical polarization state. We rotated the half wave plate from 0° to 360° with one degree step and detect the intensity by the detector Field Master GS (Coherent, s.n.: 0438B08) with the silicon detection head LM-2VIS (Coherent, s.n.: 0120B08R).

We carry out the simulation of half wave plate behavior by multiplying the matrix of linear polarizer (5), retarder (7) and the input polarization state. The equation for this model has the form of

$$\text{Fit}_{\text{HWP}} = a + b \cdot \sin^2(\alpha + c), \quad (16)$$

where a , b , c are the fit parameters and α is the angle of rotation of wave plate.

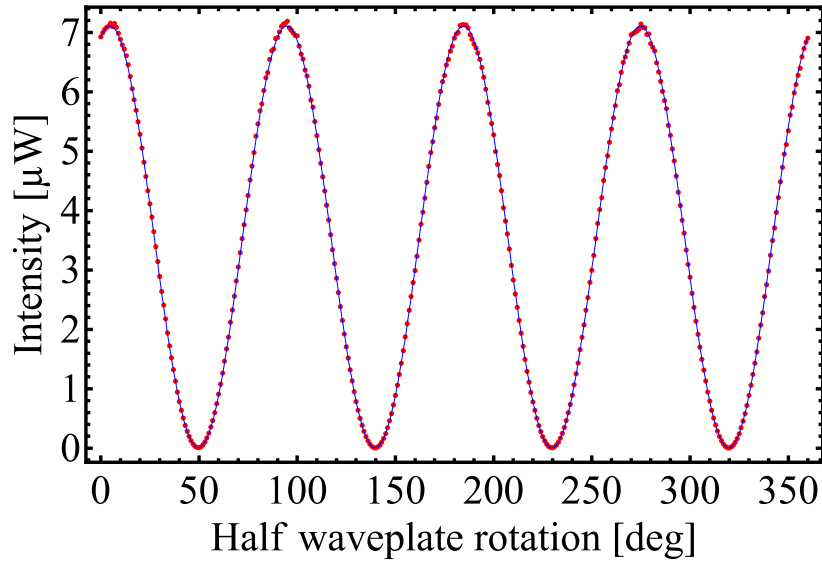


Figure 6: The intensity dependence on the rotation the half wave plate. Blue points symbolize the measured data and the red curve is the theoretical model.

The Figure 6 shows the intensity dependence on the rotation the half wave plate. Blue points symbolize our measured data and the theoretical model is represented by the red curve. We compared our measure data with the equation (16) and we found the values of constants: $a = 0.007\mu W$, $b = 7.099$ and $c = 40.317^\circ$, where the constant a comes up to noise that we measured before half wave plate was inserted into the setup. The constant b is the scaling factor of fit height. The most important is the constant c . When we rotated the half wave plate by the angle 40.317° , we get the unchanged polarization state. We can summarize that our measured data agree with the theoretical model and we can use the half wave plate to set the arbitrary linear polarized state of the input beam in our experimental setup.

3.2 Beam splitter characterization

There were two BSs cubes with length of side 25 mm at our disposal. According to the supplier the splitting ratio should be $50/50 \pm 3\%$. We want to verify the value of splitting ratio and choose the best suitable BS for the MZ interferometer. The goal of this measurement is to find the splitting ratio of the BS in dependence on the linear polarization state of light.

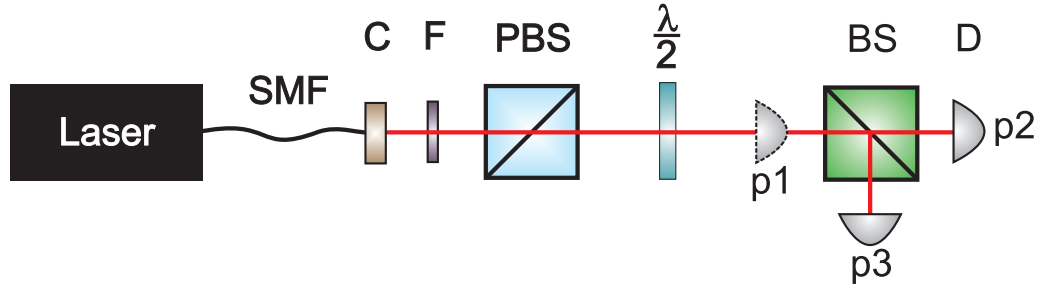


Figure 7: SMF - single mode optical fiber, C - coupler, F - filter, PBS - polarized beam splitter, $\frac{\lambda}{2}$ - half wave plate, p1, p2, p3 - positions of the detector, BS - measured beam splitter, D - detector.

The Figure 7 shows our experimental setup for measuring the splitting ratio of the BS. We use the same source of linearly polarized light and the same detector as for the half wave plate calibration. The laser beam is focused into center of the BS (Optida, OPT100603MS2) and the detector is situated 5 cm from the BS to guarantee the same width of spot in each position. We have to control this parameter because the active surface of the detector head is slightly sensitive to the width of the measured beam.

We set the zero angle of the half wave plate and measure the intensity of the laser beam in three positions p1, p2 and p3. We measure in position p1 again to ensure that the value of the intensity do not change during our measurement step. We rotate the half wave plate by 5 degrees from 0° to 45° and repeat the whole process. The measured results are in Table 2.

$\lambda/2$ [deg]		0	5	10	15	20	25	30	35	40	45
BS1	$ t ^2$	0.55	0.55	0.55	0.56	0.56	0.56	0.57	0.57	0.57	0.57
BS2	$ t ^2$	0.55	0.55	0.55	0.56	0.56	0.56	0.57	0.57	0.57	0.57

Table 2: The transmission $|t|^2$ of the BS_1 and BS_2 dependence on the input polarization state. The horizontal polarized state is symbolized by 0° and 45° symbolizes the vertical polarized state of the input beam.

Table 2 clearly shows that both measured BSs have the same splitting ratio. We reach the splitting ratio 45/55 for the horizontal polarization state and 43/57 for the vertical polarization state. We choose to use the BS_1 in our experimental setup.

The splitting ratio influences the visibility of the MZ interferometer. According to the theory we can always expect the unity visibility in the first output port. The visibility in the second output port is changed according to splitting ratio of the BS and we can expect

the maximum value of 98% for the horizontal polarization state and 96% for the vertical polarization state.

3.3 Mach-Zehnder interferometer

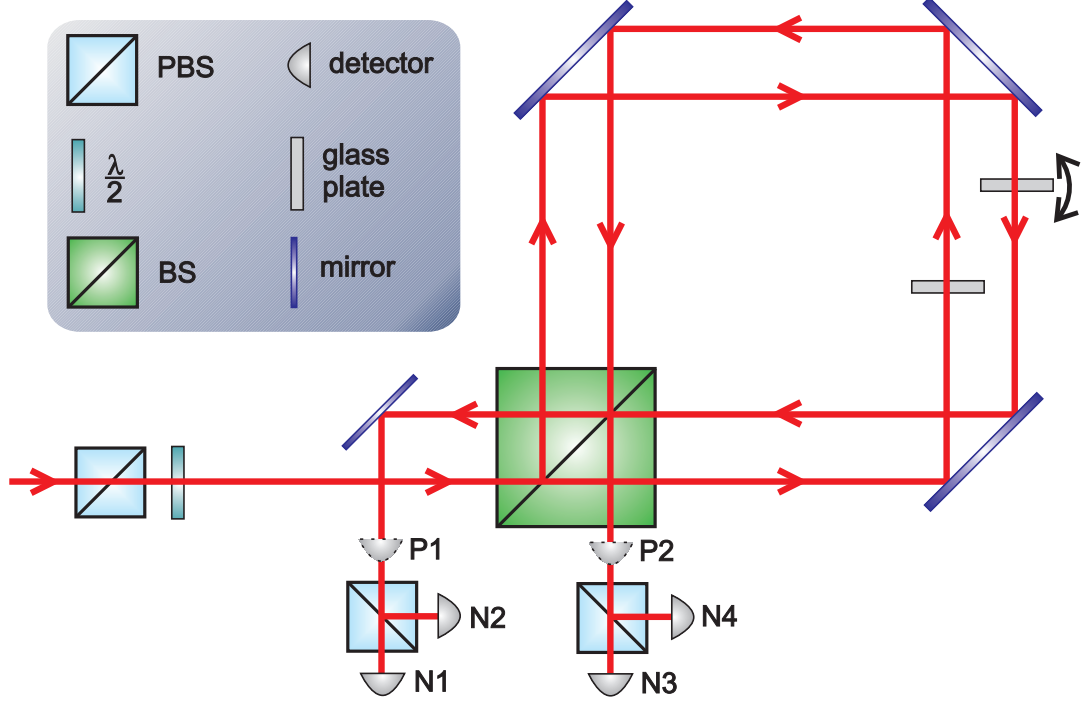


Figure 8: Our experimental realization of the MZ interferometer using displaced Sagnac construction. P1, P2 - the first and the second bulk output port, N1, N2, N3, N4 - output ports, where the beam is coupled into single mode optical fibers.

Our experimental realization of the MZ interferometer using displaced Sagnac construction is shown in the Figure 8. We use this construction to ensure the longest passive phase stability as possible. The setup is divided into three parts - the preparation of the input linear polarization state, the MZ interferometer and the detection part.

The preparation part consists of the PBS and half wave plate, where we prepare the arbitrary linear polarization state.

The MZ interferometer consists of the BS, three mirrors and two glass plates. Beams are displaced about 8 mm in the MZ interferometer. This distance was chosen as a reasonable trade - off between available clear aperture of the components and convenient individual addressing of the beams. We use the BS cube with 25 mm side length and standard 1 inch mirrors. The MZ interferometer is characterized by the visibility. To reach the

maximum and minimum intensity in one output port we employ glass plates. Glass plates are custom made (VOD Turnov) with thicknesses of 1 mm and antireflection coating at 814 nm wavelength. The first glass plate is tilted to induce a correct phase shift and the second one is fixed. The fixed glass plate is placed in the MZ interferometer to set approximately the same optical path in both interferometer arms.

The third part is the detection part. We detect intensity in output ports P1 and P2. We also detect the intensity after PBSs where the beam is coupled into single mode optical fibers (Nufern, HP780) in each output ports N1 - N4.

We use the same source of the linearly polarized light and detector as we used for the half wave plate calibration. The beam goes through the preparation part where desired linear polarization state is prepared. The beam is divided at the BS and passes through the MZ interferometer. The both beams meet together in the BS where they interfere. We detect the intensity in each output ports. We place the detector in the one port. We tilt the glass plate in the MZ interferometer and change the phase to get the maximum and minimum intensities. Than we calculate the visibility according to the equation (11). We repeat this process for both output ports and for different polarization input states.

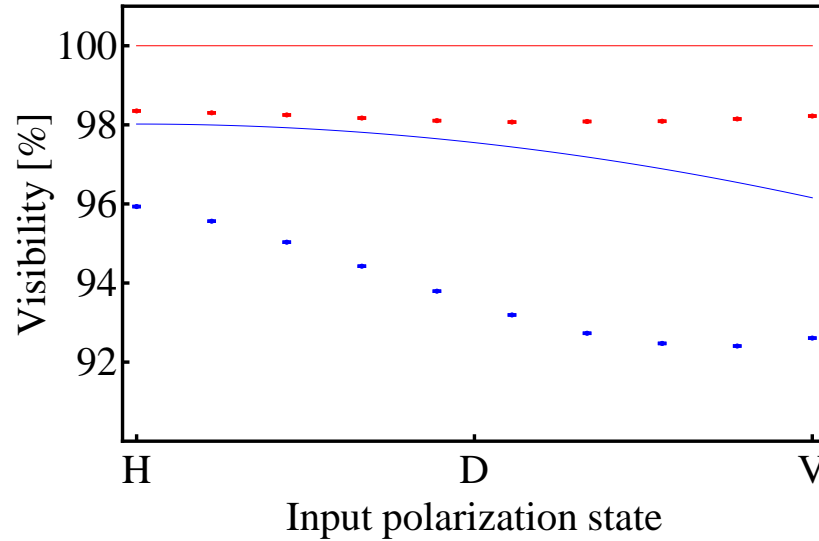


Figure 9: The visibility dependence on the input polarization state. The description on the x-axes means, H (0°) is horizontal, D ($22,5^\circ$) is diagonal, V (45°) is vertical polarization state. The first output port P1 is characterized by the red color and the second output port P2 is characterized by blue color. Curves symbolize the theoretical values of visibility and points stand for the measured values of the visibility with error bars of one standard deviation.

The visibility dependence on the input polarization state is in the Figure 9. The red curve is the theoretical prediction of the visibility in the first output port P1 and the blue curve is the theoretical prediction of the visibility in the second output port P2. Red points show the measured visibility in the first output port P1 and blue points are measured visibility in the second output port P2. Points in Figure 9 include the error bars of one standard deviation.

Measured data in the first output port P1 correspond well with the shape of the theoretical prediction. The measured visibility is lower less 2% then the theoretical values. The measured visibility in the second output port P2 are 2% lower for the horizontal and 3% lower for the vertical polarization state with the theory comparison. The shape of the theoretical prediction and measured values in the second output port P2 is different in the area of diagonal polarization state. This discrepancy can be caused by changing of the polarization state on optical elements (reflections from mirrors in the MZ interferometer). The theoretical and measured values of visibility in bulk are summarized in the Table 3. According to the theory we expect the unity visibility in the first output port P1 for both polarization states and 98% visibility for horizontal, 96% visibility for the vertical polarization state in the second output port P2.

	Theoretical visibility [%]		Visibility in bulk [%]	
Port	H	V	H	V
P1	100	100	98.35 ± 0.03	98.22 ± 0.13
P2	98	96	95.93 ± 0.05	92.61 ± 0.04

Table 3: The visibility dependence on the input polarization state in the bulk.

The difference between measured and theoretical values of visibility is mainly caused by the spatial overlap. Therefore we use coupling into single mode optical fibers (SMFs) which act as the spatial filter. The theoretical and measured values of the visibility with the aid of coupling in to the SMFs are in the Table 4.

Theoretical visibility [%]				Visibility in SMF [%]			
Port	H	Port	V	Port	H	Port	V
N1	100	N2	100	N1	99.96 ± 0.01	N2	99.98 ± 0.01
N3	98	N4	96	N3	97.33 ± 0.03	N4	93.42 ± 0.04

Table 4: The visibility dependence on the input polarization state using SMFs as spatial filter.

The Table 4 clearly shows, that values of visibility are near theoretical values. We reach more than 99.9% visibility for both polarization states in output ports N1 and N2. There are more than 97% visibility for the horizontal polarization state in the output port N3 and more than 93% for vertical polarization state in the output port N4. We reach nearly the theoretical values of visibility thanks to spatial filtration with SMFs.

3.4 Long-time phase stability

The long-time phase stability is one of the criteria of the MZ interferometer. The phase stability is affected by air fluctuations, mechanical vibrations or temperature changes.

We measured the long-time phase stability using the following procedure. We set the phase of the interferometer so that the interference minimum is in the first output port P1 and start to check the intensity by detector DET 36A/M (Thorlabs) every second for six hours. At the same time we also control the stability of the source by reference detector DET 36A/M. Measured values of intensity were logged by PicoLog1216 (PicoTech) into the computer. We corrected the measured data in the first output port P1 for the time fluctuation of the source intensity. We process the corrected data with both methods mentioned in Chapter 2.5.

The Allan variance shows how long we have to execute one particular measured step with the least affection of the noise. The length of the measure step should correspond to minimum of Allan variance.

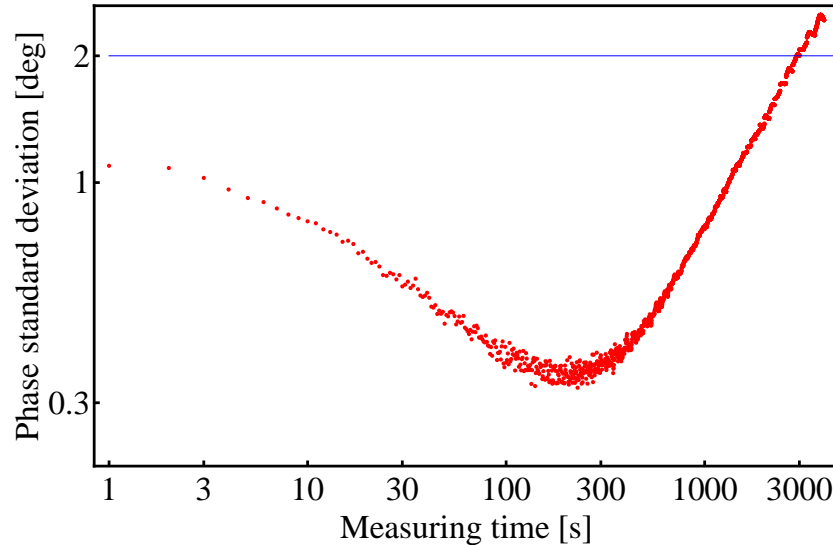


Figure 10: The dependence phase standard deviation on the time. The corrected data was evaluated using the Allan variance.

The Figure 10 shows corrected data processed by Allan variance. The minimum of Allan variance correspond to 250 seconds. It means, the measured step should take 250 seconds to be the least affected by noise. If phase standard deviation up to 2 degrees is acceptable in our experiment than the total measurement time should not exceed 2500 seconds.

The AMD method shows how phase standard deviation will maximally shift in the specific time interval.

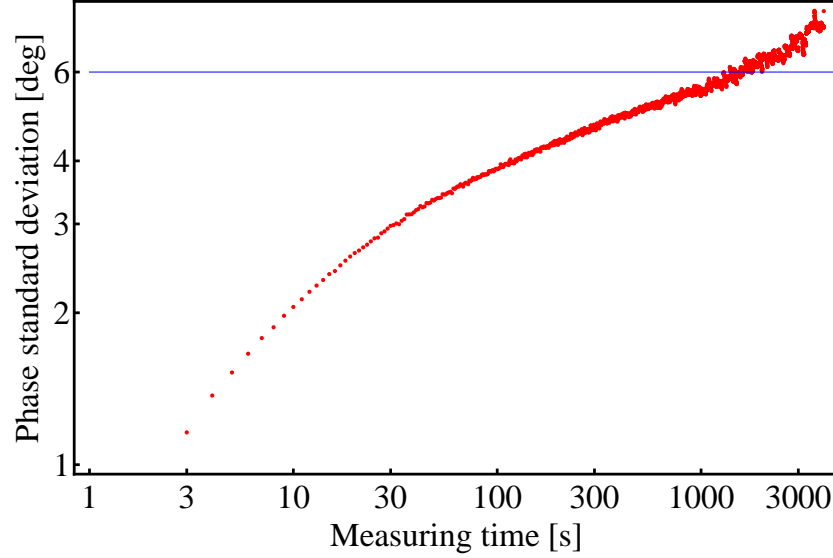


Figure 11: The dependence of the maximum phase change on the length of measurement. The corrected data were evaluated using the AMD method.

The Figure 11 shows our corrected data processed by the AMD method. The maximum deviation corresponds to three standard deviations. When we measure during 2500 seconds the phase standard deviation will shift about 6 degree which is comparable with results achieved using the Allan variance.

We reached the similar results employing the Allan variance and the AMD method. The interferometer is stable during 2500 seconds with the phase standard deviation below 2 degrees. The long stability is caused by unique construction using displaced Sagnac architecture. The both beams in the interferometer goes through same components and they register the same fluctuation of the phase. It is the reason why the interferometer is the phase stable for a long time.

4 CONCLUSION

We experimentally realized the MZ interferometer using displaced Sagnac construction and characterized it by visibility and its phase stability.

We investigated the visibility dependence on the input polarization state. According to the theory we would expect the unity visibility in the first output port and visibility of 98 % for the horizontal and 96 % for the vertical polarization state in the second output port. We reached more than 98 % for both polarization states in the first output port. In the second output port we achieved visibility of 96 % and 93 % for the horizontal and the vertical polarization state, respectively. Employing spatial filtering using single mode optical fiber we reached more than 99.9 % for both polarization states in the first output port and more than 97 % for the horizontal and more than 93 % for the vertical polarization state in the second output port. The phase stability of the realized MZ was 2500 second for the phase shift standard deviation lower than 2 degrees.

We built the ultra stable MZ interferometer with visibility very close to the theoretical values. This interferometer will be used as a part of the Toffoli gate.

5 APPENDIX

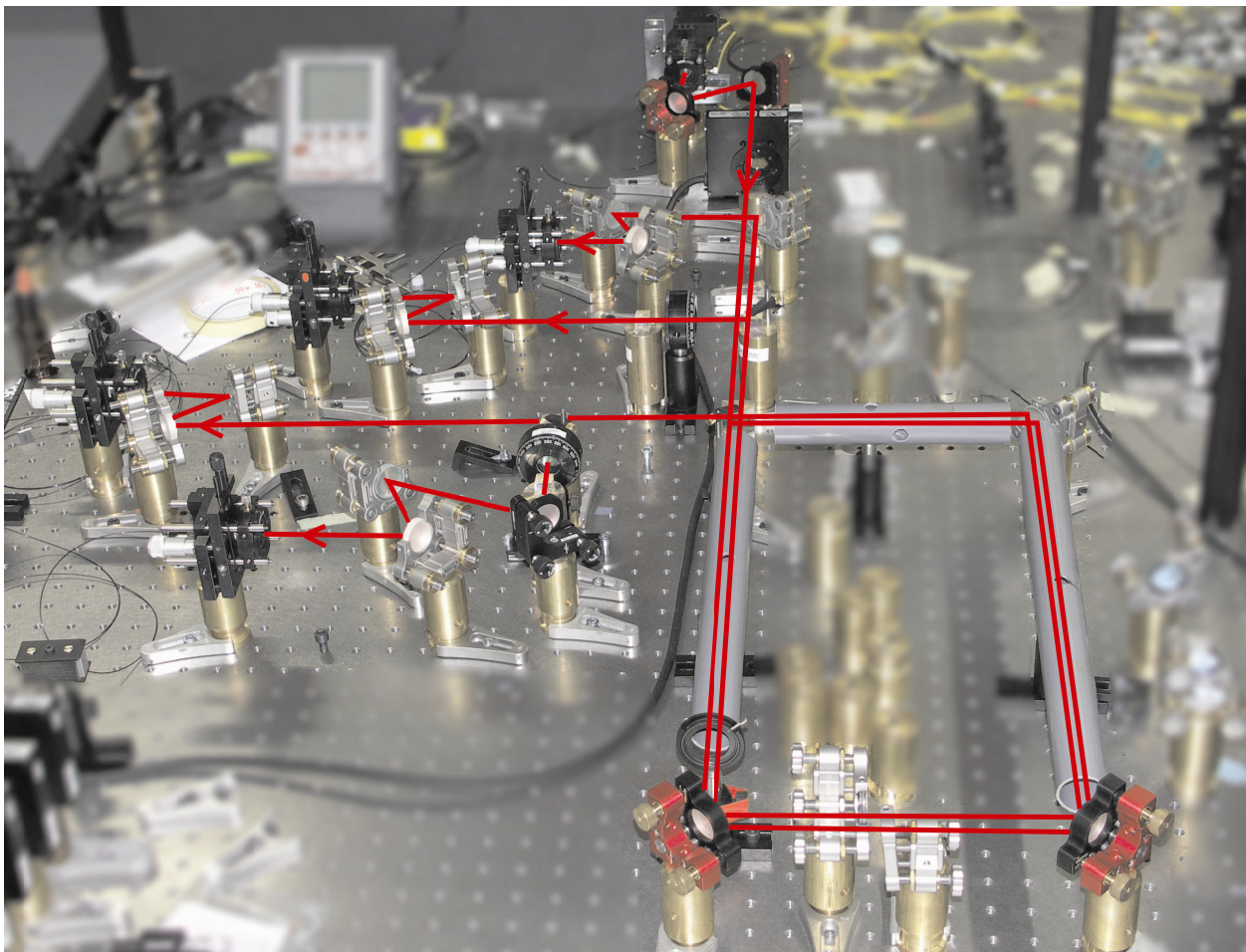


Figure 12: Photo of the experimentally realized MZ interferometer. Red lines emphasize the beam.

References

- [1] J. -P. Monchalin, M. J. Kelly, J. E. Thomas, N. A. Kurnit, A. Szöke, F. Zernike, P. H. Lee, A. Javan, *Accurate laser wavelength measurement with a precision two-beam scanning Michelson interferometer*, Appl. Opt. **20**, 736 (1981).
- [2] T. L. Gustavson, P. Bouyer, M. A. Kasevich, *Precision Rotation Measurements with an Atom Interferometer Gyroscope*, Phys. Rev. Lett. **78**, 11 (1997).
- [3] A. P. F. Turner, *Biosensors – Sense and Sensitivity*, Science **290**, 1315 (2000).
- [4] A. Ahn, Ch. Yang, A. Was, G. Popescu, Ch. Fang-Yen, K. Badizadegan, R. R. Dasari, M. S. Feld, *Harmonic phase-dispersion microscope with a Mach-Zehnder interferometer*, App. Opt. **44**, 1188 (2005).
- [5] P. G. Kwiat, J. R. Mitchell, P. D. D. Schwindt, A. G. White, *Grover’s search algorithm: an optical approach*, J. Mod. Opt. **47**, 257 (2000)
- [6] R. C. Jones, *A New Calculus for the Treatment of Optical Systems*, J. Opt. Soc. Am. **31**, 488 (1941).
- [7] M. Born and E. Wolf, *Principles of optics* (Cambridge University Press, 1997).
- [8] D. W. Allan, *Statistics of atomic frequency standards*, Proceedings of the IEEE **54**, 221 (1966).